Affinity maturation of cross-reactive CR3022 antibody against the receptor binding domain of SARS-CoV-2 via *in silico* site-directed mutagenesis

Amartya Pradhan
Netaji Subhas University of Technology, New Delhi, India; Tata Institute of Fundamental Research, Mumbai, India https://orcid.org/0000-0001-7575-8404
Samvedna Saini
Netaji Subhas University of Technology, New Delhi, India https://orcid.org/0000-0002-3374-2970
Manusmriti Agarwal
Netaji Subhas University of Technology, New Delhi, India https://orcid.org/0000-0002-9356-5857
Yatender Kumar (yatender.kumar@nsut.ac.in)
Netaji Subhas University of Technology, New Delhi, India https://orcid.org/0000-0002-9835-9892

Research Article

Keywords: antibody affinity maturation, hotspot mutation, SARS-CoV-2, molecular dynamics simulations, antigen-antibody interaction

Posted Date: October 15th, 2020

DOI: https://doi.org/10.21203/rs.3.rs-92745/v1

Abstract

Background: The coronavirus disease 2019 (COVID-19) has unequivocally affected the lives of people across the planet and has imposed an unprecedented burden on our healthcare systems. With no potent regimen for treatment, there is a dire need for finding promising candidates. Receptor binding domain (RBD) of the spike protein of severe acute respiratory syndrome coronavirus 2 (SARS-CoV-2), the causative agent of COVID-19, has proven to be a promising target owing to its role in viral invasion.

Methods: Our study aimed at generating antibody candidates from the human antibody CR3022 (derived from convalescent SARS patient) against the RBD of SARS-CoV-2 via *in silico* affinity maturation. We optimized the paratope of the CR3022 antibody towards the RBD of SARS-CoV-2 for better binding affinity and stability, employing molecular modeling, docking, and dynamics simulations.

Results: Out of seven antibody leads generated post *in silico* site-directed mutagenesis followed by preliminary screening, antibody named SAM3 was predicted to have the highest binding affinity towards RBD. However, molecular dynamics simulation of fifty nanoseconds set the seal on SAM1 and SAM2. Both demonstrated a higher binding affinity and stability compared to other counterparts and CR3022.

Conclusion: We hypothesize that SAM1, SAM2, and SAM3 antibody candidates can bind to the RBD and potentially disrupt the viral invasion. All three antibody candidates to bind residues on the human ACE-2 binding site of SARS-CoV-2 which were not conserved from SARS-CoV. Our study calls for further *in vitro* and *in vivo* testing of SAM1, SAM2, and SAM3 candidates for COVID-19 treatment.

Key Points

- Seven mutations selected for the site-directed mutagenesis
- Antibody modeled and docked with the RBD. SAM3 demonstrated the best binding affinity with RBD. Results validated with molecular dynamics simulations.
- Devised a novel way of representing stable binding affinities.
- Designed specificity of cross-reactive CR3022 antibody to bind residues on the human ACE-2 binding site of SARS-CoV-2 which were not conserved from SARS-CoV.

1. Introduction

The coronavirus disease-19 (COVID-19), following its outbreak in late 2019, has gained a passport to spread over 200 countries and territories. World Health Organization (WHO) categorized the COVID-19 outbreak as a pandemic. Preliminary studies trace back its origin following a zoonotic transfer of a bat coronavirus to humans in Wuhan, China [1,2]. This global pandemic is caused by severe acute respiratory syndrome coronavirus 2 (SARS-CoV-2), a virus belonging to the betacoronavirus genus of coronaviridae family [3,4]. CoVs carry the largest positive sense, single-stranded RNA genome of 22 to 26 kilobases (kb), which encodes four major structural proteins viz. spike (S), nucleocapsid (N), membrane (M) and the envelope (E) protein, and other non-structural proteins (nsps) that aid in replication and translation of viral genome inside the host cells [5–8].

The S protein plays a critical role in the viral invasion and is driving current research concerning diagnosis and potential therapy of COVID-19. Therefore, it has been recognized as a promising target for vaccine development, antibody therapy, while also opening avenues for treatments that focus on inhibiting host-virus interaction and viral invasion. Evidence suggests that, SARS-CoV-2, like other CoVs, ingress the human tissues via the interaction of S protein and the angiotensin-converting enzyme-2 (ACE-2) receptor expressed on the human bronchial epithelial tissues [9–11].

Current COVID-19 therapies include convalescent plasma therapy, non-steroidal anti-inflammatory drugs (NSAIDs) and anti-viral drugs. Among these, convalescent plasma therapy represents the natural response of the immune system to the viral invasion. The infamous convalescent plasma therapy, which comprises of infusion of antibodies from previously infected patients, shows evidence of notable recoveries from COVID-19 infection [12].

A number of roadblocks hinder complete acceptance of convalescent plasma therapy efficacy. Besides, the dependence on need of compatible donors, the shared antibody response propagated by this mode of treatment achieves only limited antibody affinity maturation while covering only a fraction of the patient population [13]. This calls for the design of antibodies engineered to be target specific with maximal affinity maturation which can be produced on a large scale to meet current demands.

One of the highly characterized, CR3022 convalescent antibody, is a neutralising antibody previously isolated from a convalescent SARS-patient. It targets the receptor binding domain RBD of SARS-CoV [14]. It was found to be capable of binding to the RBD of SARS-CoV-2 as well, in a recent study by Yuan and colleagues [15], thereby indicating the presence of cross-reactive epitopes in the RBD of both SARS-CoV and SARS-CoV-2. Owing to the comparatively poor binding, there is a dire need to enhance the affinity of CR3022 towards the RBD of SARS-CoV-2.

In the present study, we have performed *in silico* affinity maturation of CR3022 convalescent antibody via site-directed mutagenesis towards the S protein RBD of SARS-CoV-2. We employ robust open-source or freely accessible software to predict mutational hotspots in CR3022 antibody and to perform molecular modeling, antigen-antibody docking. Furthermore, to analyse the temporal interaction and stability, we employed molecular dynamics simulation (MDS). Another important highlight is the new way of representing and comparing binding of antigen-antibody complexes through log(|ΔG/Kd|) plots.

2. Methods

2.1 In silico site-directed mutagenesis

The crystal structure of variable heavy and light chains of the human SARS-CoV-2 neutralizing antibody, CR3022, complexed with the RBD of S protein of SARS-CoV-2 was retrieved from RCSB Protein Data Bank (PDB ID: 6W41). All the heteroatoms and water molecules were stripped from the PDB file. RBD (antigen) and CR3022 antibody were separated from the original file. The antibody PDB file was uploaded in the HotSpot Wizard 3.0 server [16]. Essential residues were not specified in the job parameters to avoid unbiased mutation prediction. Non-essential highly mutable residues, i.e., residues of antibody molecule having reliable mutability scores between 6 and 9, which reside in the catalytic pocket or access tunnels under Functional Hot Spots tool were selected for designing mutation libraries. The probability of function tolerance was kept at a minimum of 60%. Destabilizing mutations across the mutational landscape were predicted and screened. Mutations which were predicted to cause an increase in the antigen-antibody binding affinity were identified. A second screening was applied using the mCSM-AB server [17]. PDB file of antigen-antibody complex was input along with the list of screened hotspot mutations. Mutations with a predicted increase in the binding affinity from mCSM-AB were chosen for *in silico* site-directed mutagenesis.

2.2 Molecular modeling and docking

Mutant antibodies were modeled using Repertoire Builder (previously, Kotai Antibody Builder) [18]. Heavy and light chain amino acid sequences of the antibody (including the desired point substitution mutation) were pasted into the server. PDB files of modeled antibody were obtained from Repertoire Builder. PDB files were processed through the antibody paratope prediction server, Parapred, which estimates complementarity determining region (CDR) of the antibody as per the Chothia definition [19].

All the antibody files were then processed prior to molecular docking on the HADDOCK 2.4 server. Heavy and light chains were renamed as H and L, respectively. Unique residue numbers were assigned across the H and L chains using Swiss PDB Viewer [20]. Antigen residues that interact with the antibody were predicted using the EpiPred server [21]. Processed PDB files of antigen and antibody were input into the HADDOCK 2.4 server. Predicted paratopes and epitopes were specified as active site residues prior to directed docking. All docking jobs were run with default restraint settings. Best models of highest-ranked clusters were chosen for further procedure and analysis.

2.3 Molecular dynamics simulations

To analyse interaction trajectory of the docked complexes, MDS were performed. Assisted Model Building Using Energy Refinement 18 (AMBER 18) modules were used for this study [22,23]. Antigen-antibody complexes were parameterized in the terminal interface LEaP (tLEaP) using GAFF and ff14SB force fields, TIP4PBOX periodic water box with 12.0 angstroms (Å) cut off distance between the complex and periodic boundaries [24,25]. Chloride ions were added to neutralize the system. Energy minimizations were carried out for 2000 steps with first 500 steps employing the steepest descent algorithm, and later 1500 steps employing the conjugate gradient algorithm. All simulations were run with the time step of 2 femtoseconds (fs) and supported via Langevin dynamics for temperature control. All covalent bonds involving hydrogen atoms were constrained using the SHAKE algorithm throughout the simulation [26]. The system was heated from 0 K to 300 K for 20 picoseconds (ps) through the NVT ensemble. Equilibration and production runs were carried out in NPT ensemble (T = 300 K and P = 1 atm) for 1 nanoseconds (ns) and 50 ns, respectively. MD trajectories were plotted using UCSF Chimera and CPPTRAJ modules [27,28].

2.4 Antigen-antibody interaction analysis

Binding affinity (ΔG) and dissociation constant (Kd) of each antigen-antibody complex were predicted using protein-protein Protein Binding Energy Prediction (PRODIGY) server [29]. For each complex, interacting residues, along with number of interfacial contacts (IC) and percentage of non-interacting surface (NIS) were also predicted using the PRODIGY server. Interactions were visualized in LigPlot+ v2.2 and UCSF Chimera 1.14 [27,30].

3. Results And Discussions

3.1 Hotspot mutation analysis

SDM remain at core for *in silico* affinity maturation of antibodies. Six highly mutable (reliable mutability scores between 6 and 9) functional hotspots in active site and access tunnels of CR3022 (also referred as wild type, or WT) were identified using HotSpot Wizard 3.0. Binding of an antibody is mediated via CDR. Hence, mutations in CDR, and the supporting framework region (FR) shall contribute to changes in binding affinity. In this study, identified highly mutable residues lied in FR of heavy (H-FR) and light chains (L-FR). Met40 and Gly44 of H-FR2, Lys45 and Gln48 of L-FR2, Val89 and Val91 of L-FR3 were selected for designing mutational landscape libraries (Table 1). The probability of function tolerance was kept at 60% (above the default 50%). L-K45A, L-K45Q, L-K45H, L-K45M, L-K45S, L-K45W, L-Q48F, L-Q48W, L-Q48Y, and L-V91I were predicted as stabilizing mutations from mutational landscape libraries. These mutations were input along with WT antibody-antigen complex on the mCSM-AB server. Mutations L-K45A, L-K45Q, L-K45S, L-K45W, L-Q48F, L-Q48W, and L-Q48Y were predicted by mCSM-AB to increase binding affinity (ΔΔG<0) of the antigen-antibody complex (Table 2). These mutations were incorporated into WT antibody sequences to obtain the mutant antibody sequences, *viz*., SAM1, SAM2, SAM3, SAM4, SAM5, SAM6, and SAM7 with mutations L-K45A, L-K45Q, L-K45S, L-K45W, L-Q48F, L-Q48W, and L-Q48Y, respectively.

3.2 Antigen-antibody molecular modeling and docking

All the mutant antibodies were modeled using Repertoire Builder. It is one of most widely used freely accessible server for antibody modeling. Schritt et al. reported that Repertoire Builder models have lower superimposition RMSD values with respect to experimentally derived structures when compared to other alternatives [18]. To study the antigen-antibody interaction, a docking studies of RBD and candidate antibodies were carried out using HADDOCK 2.4 server. Active site residues of RBD and candidate antibodies were predicted via EpiPred and Parapred servers, respectively. Tyr19, Gly84, Lys85, Asp88, Tyr89, Tyr121, Leu123, Phe124, Arg125, Lys126, Ser127, Asn128, Lys130, Pro131, Phe132, Glu133, Arg134, Asp135, Ile136, Ser137, Glu139, Ile140, Tyr141, Gln142, Ala143,

Asn155, Cys156, Tyr157, Phe158, and Gln161 of RBD were predicted to bind CDRs of all corresponding mutant antibody candidates. Furthermore, Gly24, Ser25, Gly26, Tyr 27, Gly28, Phe29, Ile30, Thr31, Tyr32, Trp33, and Ile34 of H-CDR1; Ile43, Ile44, Tyr45, Pro46, Gly47, Asp48, Ser49, Glu 50, Thr 51, and Arg52 of H-CDR2; Ala90, Gly91, Gly92, Ser93, Gly94, Ile95, Ser96, Thr97, Pro98, Met99, Asp100, Val101, Trp102, and Gly103 of H-CDR3; Asn22, Cys23, Lys24, Ser25, Ser26, Gln27, Ser28, Val 29, Leu30, Tyr31, Ser32, Ser33, Ile34, Asn35, Tyr36, Leu37, Ala38 , Trp39 , and Tyr40 of L-CDR1; Ile52, Tyr53, Trp54, Ala54, Ser55, Arg56, Glu57, Ser58, Gly59, and Val60 of L-CDR2; Tyr89, Cys90, Gln91, Gln92, Tyr93, Tyr94, Ser95, Thr96, Pro97, Tyr98, Thr99, Phe100, and Gly101 of LCDR3, of mutant antibody candidates were predicted to bind RBD of S protein.

After retrieving the docked complex of RBD & candidate antibodies from HADDOCK 2.4, complexes were further evaluated by PRODIGY (protein-protein) for prediction of protein binding affinity (i.e. ΔG) (Table 3) and for comparison using log(|ΔG/Kdl) plots (Figure 1). For WT complex (6W41) the binding affinity is -15.2 kcal/mol with Kd of 1.80E-11 M at 37°C (log(|ΔG/Kdl) = 11.93). After *in silico* mutagenesis and screening, SAM3 was reported to have improved binding affinity of -15.8 kcal/mol and Kd of 7.10E-12 M (log(|ΔG/Kdl) = 12.35). Interestingly, the number of interfacial contacts (ICs) within the threshold distance of 5.5 Å between charged-charged, charged-polar, charged-apolar, polar-polar, polar-apolar and apolar-apolar has increased for all seven mutant antibodies when compared with WT (Figure 4; Supplementary Information, Appendix 1). However, the percent fraction of charged-non-interacting surface (NIS) has dipped for all mutant antibody complexes as compared to WT, which further indicates the involvement of hydrophobic interaction (Figure 4; Supplementary Information, Appendix 1). While, apolar-NIS percentage has spiked from 35.37% to 38.02% for SAM3 (Figure 4; Supplementary Information, Appendix 1).

3.3 Molecular dynamics simulation

To analyse temporal stability of the docked RBD-antibody complexes, molecular dynamics simulations (MDS) were carried out for 50 ns using AMBER 18 software package. Throughout the simulation, all the RBD-antibody complexes remained in bound conformation, at the center of the periodic box and away from the periodic boundaries. MD trajectories for each simulation were analyzed using root mean square deviation (RMSD) and root mean square fluctuation (RMSF) plots of backbone carbon-alpha (Cα) atoms with reference to initial conformation of production run (Figure 2 and 3). Except SAM5, RMSD plots of all antigen-mutant antibody complexes reached a near plateau after approximately 35 ns of simulation indicating conformational stability. 6W41 (CR3022), SAM1, SAM2, SAM3, SAM4, SAM5, SAM6, and SAM7 had an average RMSD value (Å) of 2.15, 4.32, 5.72, 5.08, 5.45, 10.30, 3.74, and 5.92, respectively, in the last 15 ns of the production run (Figure 2). Furthermore, average RMSF values (Å) of 6W41, SAM1, SAM2, SAM3, SAM4, SAM5, SAM6, and SAM7, were 1.61, 1.77, 1.94, 2.18, 1.92, 3.93, 1.76, and 2.16, respectively (Figure 3). SAM5 is the most flexible complex with the highest fluctuation values indicating the lowest stability of interacting residues. Analysis of RMSF plots of rest of the complexes revealed fair stability of interacting residues.

3.4 Antigen-Antibody Interaction Analysis

Yuan et al [31] found that despite 86% (24 out of 28) conservation of epitopes for CR3022 between SARS-CoV and SARS-CoV-2 RBD, the CR3022 antigen binding fragment (Fab) binds to the RBD of the former with a much higher affinity than to that of the latter. Their studies also underlined the absence of overlap between the epitopes and the ACE-2 binding site of the SARS-CoV-2 RBD. This implies the involvement of a neutralising mechanism, which appears to be independent of competitive inhibition or direct blocking of the receptor binding site. Furthermore, IgBLAST analysis of CR3022 carried out by them revealed that its immunoglobulin G heavy-chain variable (IGHV) region is 3.1 % somatically mutated leading to 8 amino acid changes with respect to the germline sequence, while its IG light-κ-chain variable (IGKV) region was found to be only 1.3% somatically mutated with 3 amino acid changes with respect to the germline. 6 out of these 11 mutations were part of the FR, indicating their significance in the affinity maturation process [31]. These findings highlight the scope of increasing the binding affinity of CR3022 through mutagenesis and the affinity maturation and the need for increasing its specificity to SARS-CoV-2 RBD, particularly the ACE-2 binding site.

SAM3 exhibits increased binding affinity pre-MDS, while SAM1 and SAM2 emerge with leading binding affinity post-MDS (Table 3 and Figure 1). All three of these antibodies are distinct from the other candidates due to possession of a single mutation in the FR of their light chain sequence. In addition, the data derived from PRODIGY on the number and types of ICs present in the complexes pre- and post-MDS in comparison with the CR3022 WT antibody complex (PDB ID: 6W41) suggests a decrease in the number of interfacial contacts of the charged-charged, charged-polar, charged-apolar and polar-polar category post-MDS, while also indicating an increase in charged-polar, charged-apolar and polar-polar type of interactions in post-MDS complexes (Figure 4). These interactions were visualized using LigPlot+ to seek concurrence (Figure 5). However, strikingly the residues substituted as part of the mutation did not form any interaction as observed in the complexes across SAM1, SAM2 and SAM3 which leads us to suppose that the mutations influenced structural change to account for formation of new interactions and the predicted increase in binding affinity. This observation along with the predicted decrease of charged residues comprising the NIS in pre-MDS as well as post-MDS complexes is indicative of potential possessed by affinity matured antibodies to build more specific interactions driven by charged residues in comparison to CR3022, the neutralisation and binding mechanism of which is largely driven by hydrophobic interactions [31]. Moreover, the three lead antibodies (SAM1, SAM2, and SAM3), in comparison to CR3022, gain interfacial contacts with residues on the S protein RBD that overlap with its ACE-2 binding site post introduction of respective mutations (Figure 4). These interactions prove to be particularly encouraging as they include those residues of the SARS-CoV-2 RBD-ACE-2 binding site that are not conserved from SARS-CoV (See Supplementary Information, Appendix 2). These observations confer the affinity matured antibodies the potential of desired specificity to SARS-CoV-2 RBD-ACE-2 binding site in comparison to originally cross reactive CR3022.

Another aspect worthy of discussion is the choice of epitopes considered in this study. While the epitopes of CR3022 were defined by Yuan et al, we chose to consider the epitopes predicted by EpiPred as part of our antibody-affinity maturation protocol for the designed mutant antibodies, as opposed to the epitopes of CR3022 stated in the literature to investigate their potential of binding to the monomer of SARS-CoV-2 RBD in the absence of any steric hindrance or exclusion posed by rest of the homotrimer. These predicted epitopes happened to overlap with ACE-2 binding site residues of the SARS-CoV-2 RBD. Upon directed docking with the aforementioned epitopes, the resultant docked complexes with high binding affinities displayed interaction that proposed competitive inhibition of ACE-2 binding site on SARS-CoV-2 as their potential mechanism of action. Docking of the designed antibodies that differed from the

wild type at only a single residue, directed towards desired epitopes indicates probable potential for direct blocking of the ACE-2 binding site in the absence of steric hindrance from immune-evasive buried protomers of the SARS-CoV-2 S protein homotrimer as well as its S2 perfusion unit are ruled out [31].

An important aspect of our protocol was also the inclusion of the factor of the dissociation constant (Kd) in addition to Gibbs free binding energy (ΔG). ΔG value is critical in understanding how firmly the antigen binds its respective antibody. However, it does not tell about the tendency of dissociation of antigen-antibody interaction at a particular temperature. Hence, to overcome this uncertainty, it is essential to bring Kd into the picture of binding affinity. Kd provides a quantitative measure of dissociation of a complex binding at a given temperature. Hence, we incorporated Kd to calculate binding affinities and devised a novel way visualizing and comparing the data through log(|ΔG/Kd|) bar graphs. Higher columns on log(|ΔG/Kd|) plots correspond to the better binding. Thus, log(|ΔG/Kd|) plot provide a clearer and quantitative understanding of antigen-antibody binding.

4. Conclusion

In this study we performed the affinity maturation of CR3022 convalescent antibody towards S protein RBD of SARS-CoV-2. Three antibody candidates, *viz.* SAM1 and SAM2 (post-MDS), and SAM3 (pre-MDS) demonstrated better binding affinity compared to it counterparts and CR3022 antibody. Besides better binding affinity, they also demonstrated greater target specificity towards SARS-CoV-2 S protein RBD by virtue of blocking human ACE-2 binding site as predicted through our study. We also report a novel strategy to compare binding affinities via bar graphs showing log(|ΔG/Kd|) plots of docked antigen-antibody complexes. Since, this is a computational study, binding affinity and efficacy must be experimentally validated via *in vitro* and *in vivo* testing.

On the other hand, studies elucidating the dependence of SARS-CoV-2 on TMPRSS2 and human proprotein convertase furin for pre-activation of its immune evasive S protein into a structurally available standing up position for successful cell entry into the host [32] provide an avenue for synergistic or bispecific antibody therapies that can completely block host invasion by SARS-CoV-2. Proposed bispecific strategies that form the future aspects of our study can include simultaneous inhibition of furin as well as blocking of S protein ACE-2 binding epitopes.

Declarations

Author descriptions

Amartya Pradhan completed his Bachelor of Engineering from the Netaji Subhas University of Technology. He is currently a Junior Research Scholar at the Tata Institute of Fundamental Research, Mumbai, India. This study was a part of his undergraduate thesis project. He is also serving as the Vice President of Project Encephalon.

Samvedna Saini is a doctoral student at the Netaji Subhas University of Technology. She completed her Master of Science from Anna University, India. She was also a Junior Research Fellow of the Department of Science and Technology-Science and Engineering Research Board (DST-SERB).

Manusmriti Agarwal completed her Bachelor of Engineering from the Netaji Subhas University of Technology. This study was a part of her undergraduate thesis project. She is recipient of the membership of the American Chemical Society.

Yatender Kumar is an Assistant Professor at the Netaji Subhas University of Technology. He completed his doctoral and post-doctoral studies from the Centre for Cellular and Molecular Biology, India, and Max-Planck Unit for Structural and Molecular Biology, Germany, respectively.

Author contributions

MA and AP designed the study. SS and MA performed modeling, docking and mutagenesis. AP performed molecular dynamics simulations and prepared tables and figures. SS, MA and AP and YK analyzed the data. AP, MA, and SS prepared the manuscript. All authors read and approved the final manuscript.

Acknowledgments

This project was supported by a grant [ECR/2016/001752] awarded by the Department of Science and Technology (DST) - Science and Engineering Research Board (SERB) to YK. AP acknowledges the Supercomputing Facility for Bioinformatics and Computational Biology (SCFBio) at the Indian Institute of Technology, Delhi, for providing access to the high-performance computing servers and AMBER modules. All authors thank Prof. Sonika Bhatnagar at the Netaji Subhas University of Technology for her guidance in molecular dynamics simulations.

Conflicts of Interest

The authors declare no financial interests or conflicts of interest related to this research.

References

1. Lau SKP, Luk HKH, Wong ACP, et al. Possible Bat Origin of Severe Acute Respiratory Syndrome Coronavirus 2. Emerg. Infect. Dis. 2020; 26:
2. Wu F, Zhao S, Yu B, et al. A new coronavirus associated with human respiratory disease in China. Nature 2020; 579:265–269
3. Zhou P, Yang X Lou, Wang XG, et al. A pneumonia outbreak associated with a new coronavirus of probable bat origin. Nature 2020; 579:270–273
4. Cui J, Li F, Shi ZL. Origin and evolution of pathogenic coronaviruses. Nat. Rev. Microbiol. 2019; 17:181–192
5. Narayanan K, Ramirez SI, Lokugamage KG, et al. Coronavirus nonstructural protein 1: Common and distinct functions in the regulation of host and viral gene expression. Virus Res. 2015; 202:89–100

6. Mortola E, Roy P. Efficient assembly and release of SARS coronavirus-like particles by a heterologous expression system. FEBS Lett. 2004; 576:174–178
7. Masters PS. The Molecular Biology of Coronaviruses. Adv. Virus Res. 2006; 65:193–292
8. Fehr AR, Perlman S. Coronaviruses: An overview of their replication and pathogenesis. Coronaviruses Methods Protoc. 2015; 1–23
9. Bolles M, Donaldson E, Baric R. SARS-CoV and emergent coronaviruses: Viral determinants of interspecies transmission. Curr. Opin. Virol. 2011; 1:624–634
10. Qiu Y, Zhao YB, Wang Q, et al. Predicting the angiotensin converting enzyme 2 (ACE2) utilizing capability as the receptor of SARS-CoV-2. Microbes Infect. 2020; 22:221–225
11. Kuba K, Imai Y, Rao S, et al. A crucial role of angiotensin converting enzyme 2 (ACE2) in SARS coronavirus-induced lung injury. Nat. Med. 2005; 11:875–879
12. Casadevall A, Pirofski LA. The convalescent sera option for containing COVID-19. J. Clin. Invest. 2020; 130:1545–1548
13. Yuan M, Liu H, Wu NC, et al. Structural basis of a shared antibody response to SARS-CoV-2.
14. ter Meulen J, van den Brink EN, Poon LLM, et al. Human Monoclonal Antibody Combination against SARS Coronavirus: Synergy and Coverage of Escape Mutants. PLoS Med. 2006; 3:e237
15. Tian X, Li C, Huang A, et al. Potent binding of 2019 novel coronavirus spike protein by a SARS coronavirus-specific human monoclonal antibody. Emerg. Microbes Infect. 2020; 9:382–385
16. Sumbalova L, Stourac J, Martinek T, et al. HotSpot Wizard 3.0: web server for automated design of mutations and smart libraries based on sequence input information. Nucleic Acids Res. 2018; 46:W356–W362
17. Pires DE V, Ascher DB. mCSM-AB: a web server for predicting antibody-antigen affinity changes upon mutation with graph-based signatures. Nucleic Acids Res. 2016; 44:469–473
18. Schritt D, Li S, Rozewicki J, et al. Repertoire Builder: high-throughput structural modeling of B and T cell receptors. Mol. Syst. Des. Eng. 2019; 4:761–768
19. Liberis E, Veličković P, Sormanni P, et al. Parapred: antibody paratope prediction using convolutional and recurrent neural networks. Bioinformatics 2018; 34:2944–2950
20. Schwede T, Kopp J, Guex N, et al. SWISS-MODEL: An automated protein homology-modeling server. Nucleic Acids Res. 2003; 31:3381–3385
21. Beckervordersandforth R, Ebert B, Schäffner I, et al. Role of Mitochondrial Metabolism in the Control of Early Lineage Progression and Aging Phenotypes in Adult Hippocampal Neurogenesis. Neuron 2017; 93:560-573.e6
22. Weiner PK, Kollman PA. AMBER: Assisted model building with energy refinement. A general program for modeling molecules and their interactions. J. Comput. Chem. 1981; 2:287–303
23. Salomon-Ferrer R, Case DA, Walker RC. An overview of the Amber biomolecular simulation package. WIREs Comput Mol Sci 2012;
24. Sprenger KG, Jaeger VW, Pfaendtner J. The general AMBER force field (GAFF) can accurately predict thermodynamic and transport properties of many ionic liquids. J. Phys. Chem. B 2015; 119:5882–5895
25. Maier JA, Martinez C, Kasavajhala K, et al. ff14SB: Improving the Accuracy of Protein Side Chain and Backbone Parameters from ff99SB. J. Chem. Theory Comput. 2015; 11:3696–3713
26. Ryckaert JP, Ciccotti G, Berendsen HJC. Numerical integration of the cartesian equations of motion of a system with constraints: molecular dynamics of n-alkanes. J. Comput. Phys. 1977; 23:327–341
27. Pettersen EF, Goddard TD, Huang CC, et al. UCSF Chimera - A visualization system for exploratory research and analysis. J. Comput. Chem. 2004; 25:1605–1612
28. Roe DR, Cheatham TE. PTRAJ and CPPTRAJ: Software for processing and analysis of molecular dynamics trajectory data. J. Chem. Theory Comput. 2013; 9:3084–3095
29. Xue LC, Rodrigues JP, Kastritis PL, et al. PRODIGY: a web server for predicting the binding affinity of protein–protein complexes. Bioinformatics 2016; btw514
30. Laskowski RA, Swindells MB. LigPlot+: Multiple ligand-protein interaction diagrams for drug discovery. J. Chem. Inf. Model. 2011; 51:2778–2786
31. Yuan M, Wu NC, Zhu X, et al. A highly conserved cryptic epitope in the receptor binding domains of SARS-CoV-2 and SARS-CoV.
32. Shang J, Wan Y, Luo C, et al. Cell entry mechanisms of SARS-CoV-2. Proc. Natl. Acad. Sci. U. S. A. 2020; 117:11727–11734

Tables

Chain	Position	Residue	Ala	Arg	Asn	Asp	Cys	Gln	Glu	Gly	His	Ile	Lys	Leu	Met	Phe	Pro	Ser	Thr	Val
H	40	Met	0.8	0.4	1.4	2.3	3	0	0.2	1.7	0.8	10	0.7	0.6	-	2.9	18	1.6	6.1	9.7
H	44	Gly	1.7	-	2.8	3	2.5	4	25	-	3.2	-	6.7	15	8	5.1	9.5	3.2	8	16
L	45	Lys	-3.2	0.5	2	4.7	1.4	-1.4	0	-	-5.3	11	-	3.8	-1.5	1	-	-1.7	3.4	11
L	48	Gln	1.2	1.3	1.2	1.8	2.6	-	1.1	3	0.5	3.6	0.7	0.2	0.3	-1	-	1.9	2.1	3.3
L	89	Val	1.7	2.2	2	2.8	-	0.9	2	-	-	-	-	2	1.5	4.4	-	-	-	-
L	91	Val	2.5	2.4	3.1	3.6	4.6	1.3	2.1	-	2	-0.3	2.1	1.7	1.2	1	-	3.1	1.5	-

Table 1. Hotspot Wizard 3.0 results. Predicted stability (Kcal/mol) of designed functional hotspot mutations. All residues selected for designing library had a reliable mutability score between 6 and 9, and probability of function tolerance above 60% Destabilizing mutation are colored red whereas stabilizing mutations are colored dark green.

Chain	Wildtype Residue	Position	Mutant Residue	RSA (%)	$\Delta\Delta G_{pred}$
L	K	45	A	32.5	-0.422
L	K	45	Q	32.5	-0.482
L	K	45	H	32.5	0.475
L	K	45	M	32.5	0.107
L	K	45	S	32.5	-0.428
L	K	45	W	32.5	-0.74
L	Q	48	F	59.6	-0.354
L	Q	48	W	59.6	-0.375
L	Q	48	Y	59.6	-0.25
L	V	91	I	23.9	0.163

Table 2. mCSM-AB results. Predicted change in binding affinity ($\Delta\Delta G_{pred}$ in Kcal/mol) of stabilizing functional hotspot mutations. RSA – residue relative solvent accessibility. Seven mutations ($\Delta\Delta G_{pred} < 0$) were finalized for lead mutant antibodies, and for further analysis.

scFv	Mutation/WT	Pre-MDS		Post-MDS	
		ΔG (kcal/mol)	Kd (M) at 37.0°C	ΔG (kcal/mol)	Kd (M) at 37.0°C
6W41	WT	-15.2	1.80E-11	-10.9	2.20E-08
SAM1	K45A	-13.2	5.10E-10	-11.2	1.20E-08
SAM2	K45Q	-13.7	2.00E-10	-11.2	1.20E-08
SAM3	K45S	-15.8	7.10E-12	-9.2	3.30E-07
SAM4	K45W	-14.4	6.50E-11	-10.4	4.40E-08
SAM5	Q48F	-13.1	5.90E-10	-9.1	3.60E-07
SAM6	Q48W	-12.7	1.20E-09	-8.8	5.90E-07
SAM7	Q48Y	-12.9	7.90E-10	-8.8	5.90E-07

Table 3. Binding affinities and dissociation constant of docked antigen-antibody complexes. Binding affinities (ΔG) are measured in Kcal/mol. Dissociation constants (Kd) are measured in M at 37°C.

Figures

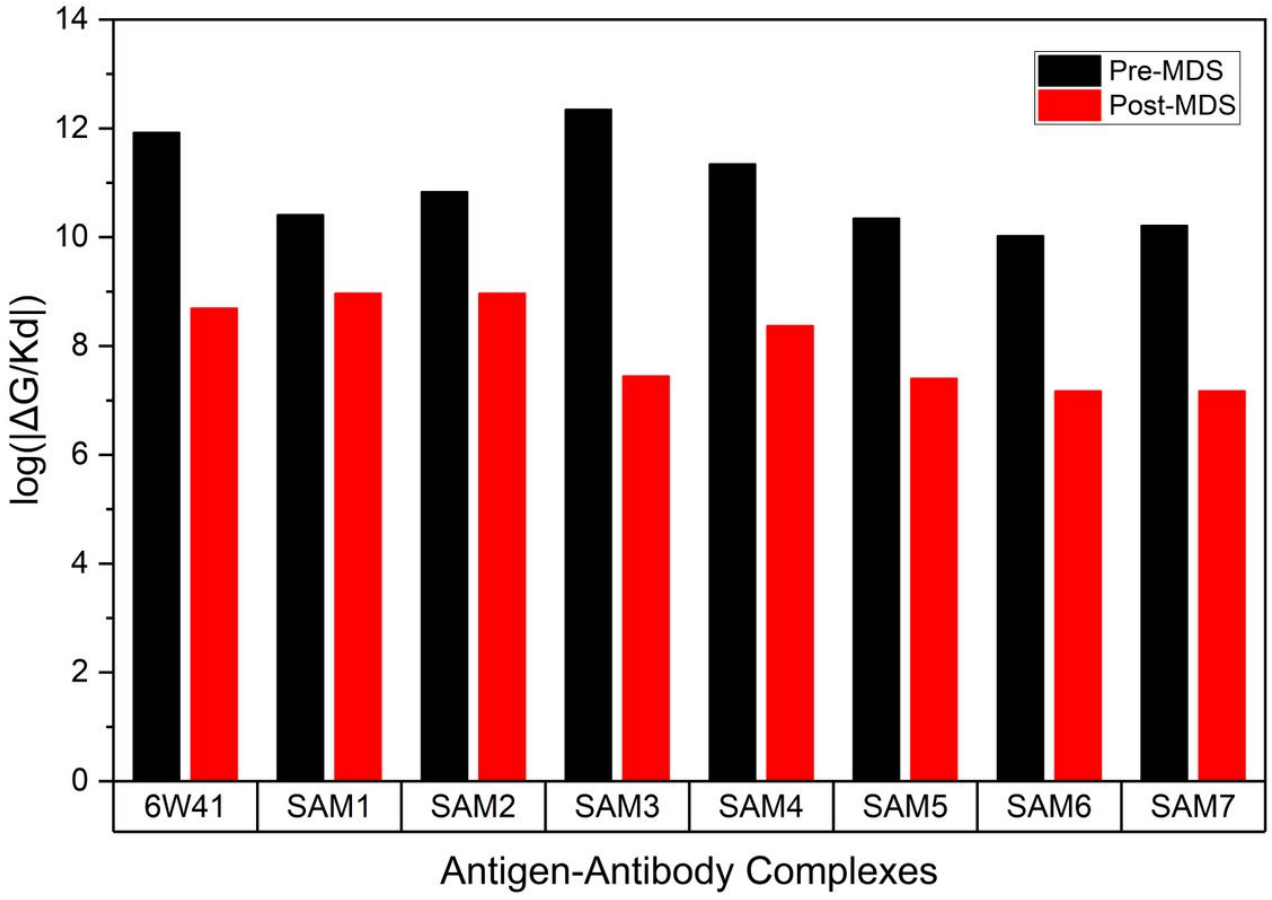

Figure 1

Bar graphs representing log(|ΔG/Kd|) values for each complex before and after molecular dynamics simulation (MDS). SAM3 (pre-MDS), and SAM1 and SAM2 (post-MDS) showed better binding affinity compared to WT antibody (6W41).

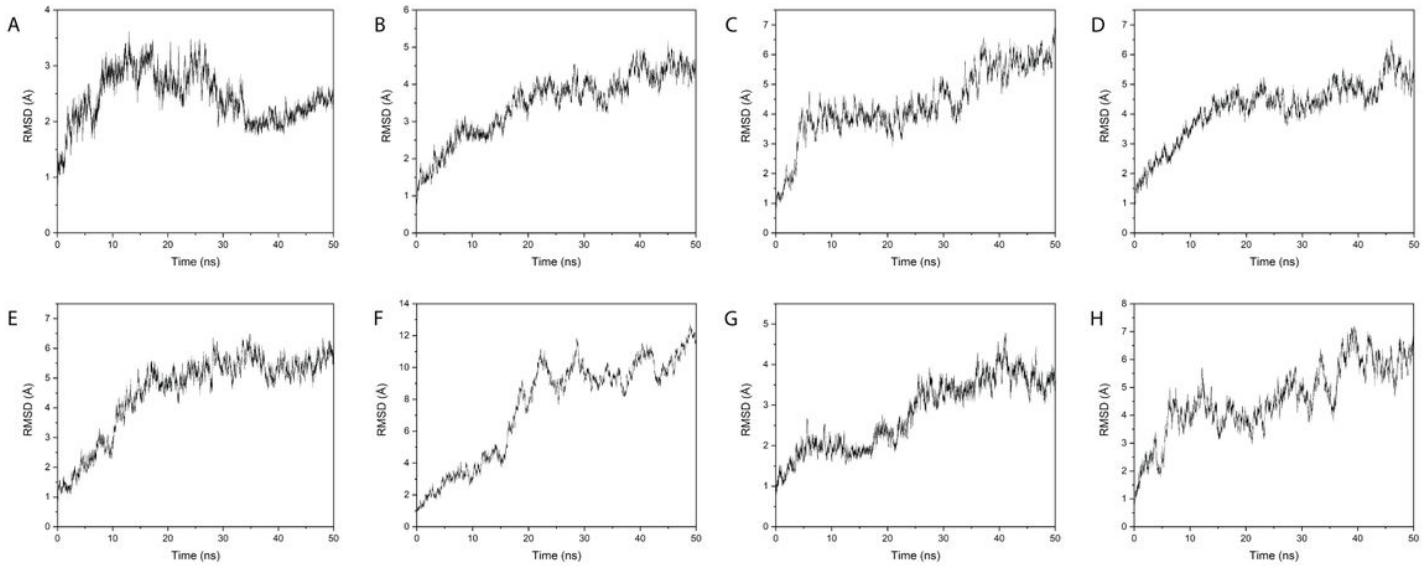

Figure 2

Root mean square deviation plots. Each plot shows RMSD (Å) values of all alpha-carbons (Cα) with reference to structure in the first frame during production run. A – 6W41; B – SAM1; C – SAM2; D – SAM3; E – SAM4; F – SAM5; G – SAM6; H – SAM7.

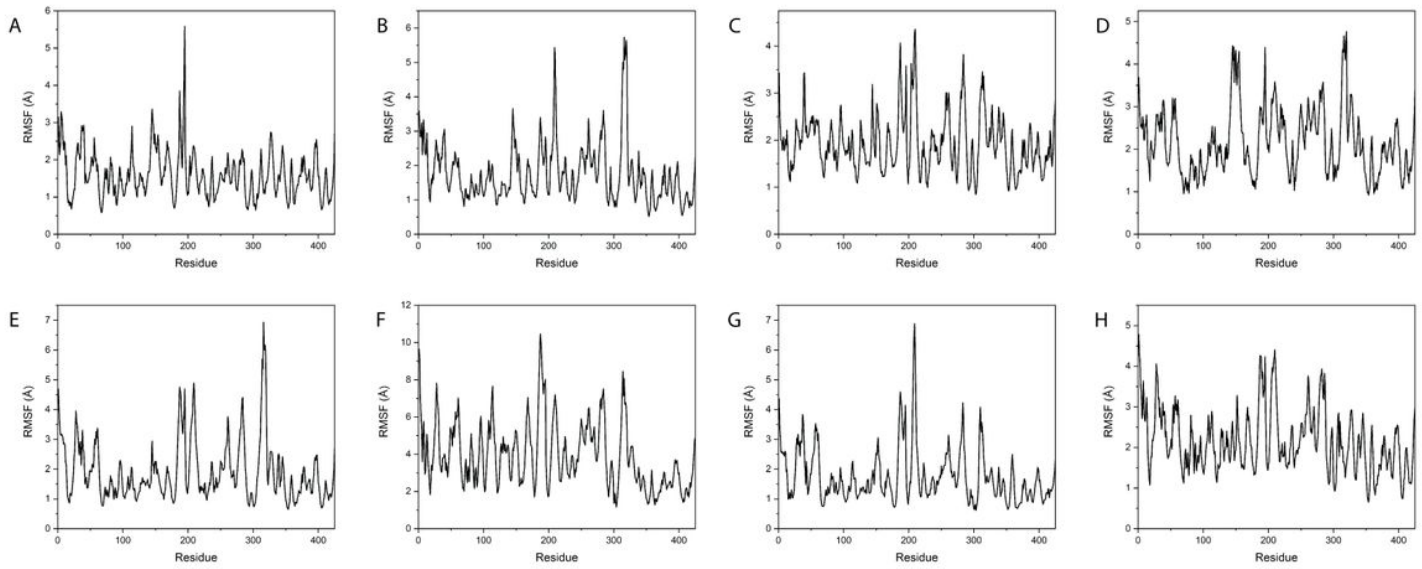

Figure 3

Root mean square fluctuation plots. Each plot shows RMSF (Å) values of each residue with reference to structure in the first frame during production run. A – 6W41; B – SAM1; C – SAM2; D – SAM3; E – SAM4; F – SAM5; G – SAM6; H – SAM7. Residues 1 to 195 are of RBD, 196 to 312 are of variable heavy chain, and 312 to 425 are of variable light chain.

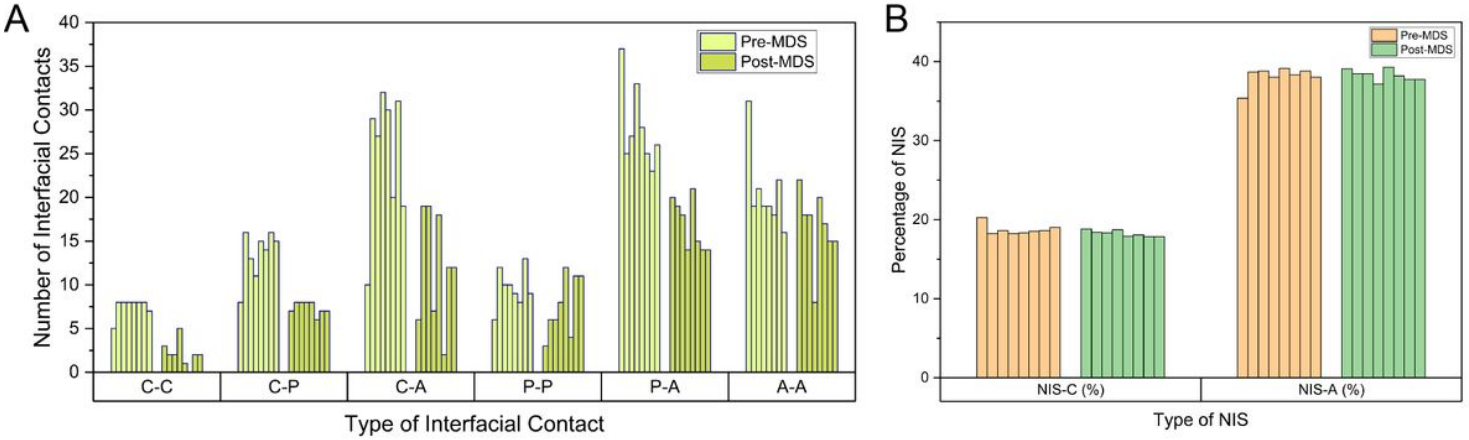

Figure 4

Antigen-antibody interaction analysis via PRODIGY server. (A) Number and type of interfacial contacts (ICs) predicted before and after MDS (left to right: 6W41, SAM1, SAM2, SAM3, SAM4, SAM5, SAM6, SAM7). ICs: charged-charged (C-C), charged-polar (C-P), charged-apolar (C-A), polar-polar (P-P), polar-apolar (P-A), and apolar-apolar (A-A). (B) Percentage of different types of non-interacting surface (NIS) predicted pre-MDS and post-MDS (left to right: 6W41, SAM1, SAM2, SAM3, SAM4, SAM5, SAM6, SAM7). NIS-C: non-interacting surface-charged; NIS-A: non-interacting surface-apolar.

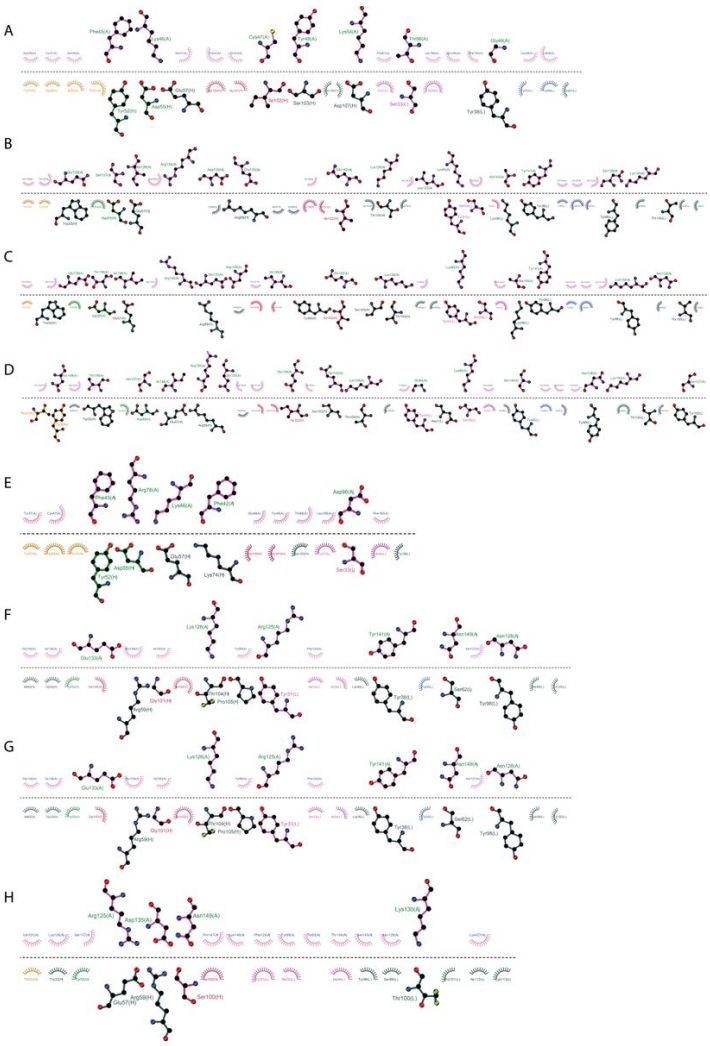

Figure 5

Visualization non-bonded interactions in antigen-antibody docked poses using LigPlot+ software. A – 6W41 (pre-MDS), B – SAM1 (pre-MDS), C – SAM2 (pre-MDS), D – SAM3 (pre-MDS), E – 6W41 (post-MDS), F – SAM1 (post-MDS), G – SAM2 (post-MDS), and H – SAM3 (post-MDS).

Supplementary Files

This is a list of supplementary files associated with this preprint. Click to download.

- SupplementaryInfoCOVIDAAM.docx